CHEMISTRY OF MATERIALS

pubs.acs.org/cm

Article

Revealing the Role of Polaron Distribution on the Performance of n-Type Organic Electrochemical Transistors

Junwei Shi,[†] Peiyun Li,[†] Xin-Yu Deng, Jingcao Xu, Zhen Huang, Yuqiu Lei, Yunfei Wang, Jie-Yu Wang, Xiaodan Gu, and Ting Lei*

Cite This: *Chem. Mater.* 2022, 34, 864−872

Read Online

ACCESS | Metrics & More | Article Recommendations | Supporting Information

ABSTRACT: Organic electrochemical transistors (OECTs) have shown great potential in bioelectronics and neuromorphic computing. However, the low performance of n-type OECTs impedes the construction of complementary-type circuits for low-power-consumption logic circuits and high-performance sensing. Compared with their p-type counterparts, the low electron mobility of n-type OECT materials is the primary challenge, leading to low μC^* and slow response speed. Nevertheless, no successful method has been reported to address the issue. Here, we find that the charge carrier mobility of n-type OECTs can be significantly enhanced by redistributing the polarons on the polymer backbone. As a result, 1 order of magnitude higher electron mobility is achieved in a new polymer, P(gPzDPP-CT2), with a simultaneously enhanced μC^* value and faster response speed. This work reveals the important role of polaron distribution in enhancing the performance of n-type OECTs.

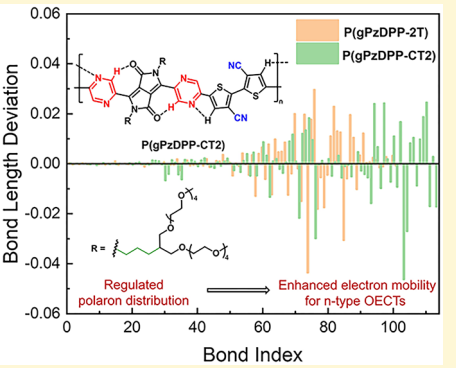

INTRODUCTION

Because of their low operation voltage, high transconductance, and good biocompatibility, organic electrochemical transistors (OECTs) have been successfully used in many areas, including chemo/biosensors, bioelectronics, and neuromorphic computing.[1−3] The past few years have witnessed the rapid development of OECTs. Various materials and different device structures have been exploited to improve the performance and expand the applications of OECTs.[4−6] Recently, thiophene-based conjugated polymers and some donor−acceptor (D−A)-conjugated polymers functionalized with ethylene glycol (EG) side chains are used as p-type OECTs.[7−10] They have shown high performances with figure-of-merit values μC^* over 200 F cm^{-1} V^{-1} s^{-1},[11,12] higher than conventional PEDOT:PSS-based OECT devices.

Compared to the diverse p-type materials and their outstanding performance, n-type OECTs lag far behind in terms of both quantity and performance.[13,14] Current n-type OECT polymers are based on two types. One is D−A polymers based on naphthalene diimide (NDI), including P(gNDI-gT2) and P-90, the other is ladder-type polymers, including BBL and PgNaN (Figure S1).[15−18] The shortage and poor performance of n-type polymers for OECTs obstruct the development of complementary metal oxide semiconductor (CMOS)-like integrated circuits. CMOS-like logic circuits can show lower power consumption than those using only the unipolar ones.[13] Recent studies also proved that CMOS-like OECT circuits could further improve the sensitivity of chemo/biosensors.[19] The enormous performance gap between p-type and n-type polymers becomes one of the biggest obstacles for the practical applications for OECT-based circuits.

To explore the potential approach to solve the low-performance issue of n-type OECT materials, we summarized the performance parameters of some n-type polymers used in OECTs (Table S1).[20] We found that although the volumetric capacitance (C^*) values of p- and n-type OECTs are at a similar level (≥100 F cm^{-3}), the charge carrier mobilities (μ) of n-type OECT polymers (10^{-4}−10^{-3} cm^2 V^{-1} s^{-1}) are several orders of magnitude lower than those of their p-type counterparts (10^{-1}−10^{1} cm^2 V^{-1} s^{-1}). In addition to μC^*, which determines transducer sensitivity, charge carrier mobility also affects the response speed of the device. The switching speed of OECTs is determined by two parts: electron transport and ion transport. For a long time, low ion mobility limited the speed of many electrochemical systems, making long response time a major challenge for the practical applications of OECTs for high-frequency signals. Recently, a type of internal ion-gated organic electrochemical transistor has been developed.[21,22] The shortened ion transport distance freed the p-type OECT device from the limitation of ion transport, and the new OECT device configuration fell into the hole/electron mobility governed region. p-Type OECT materials usually

Received: November 23, 2021
Revised: December 16, 2021
Published: January 6, 2022

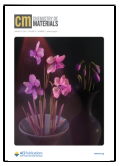

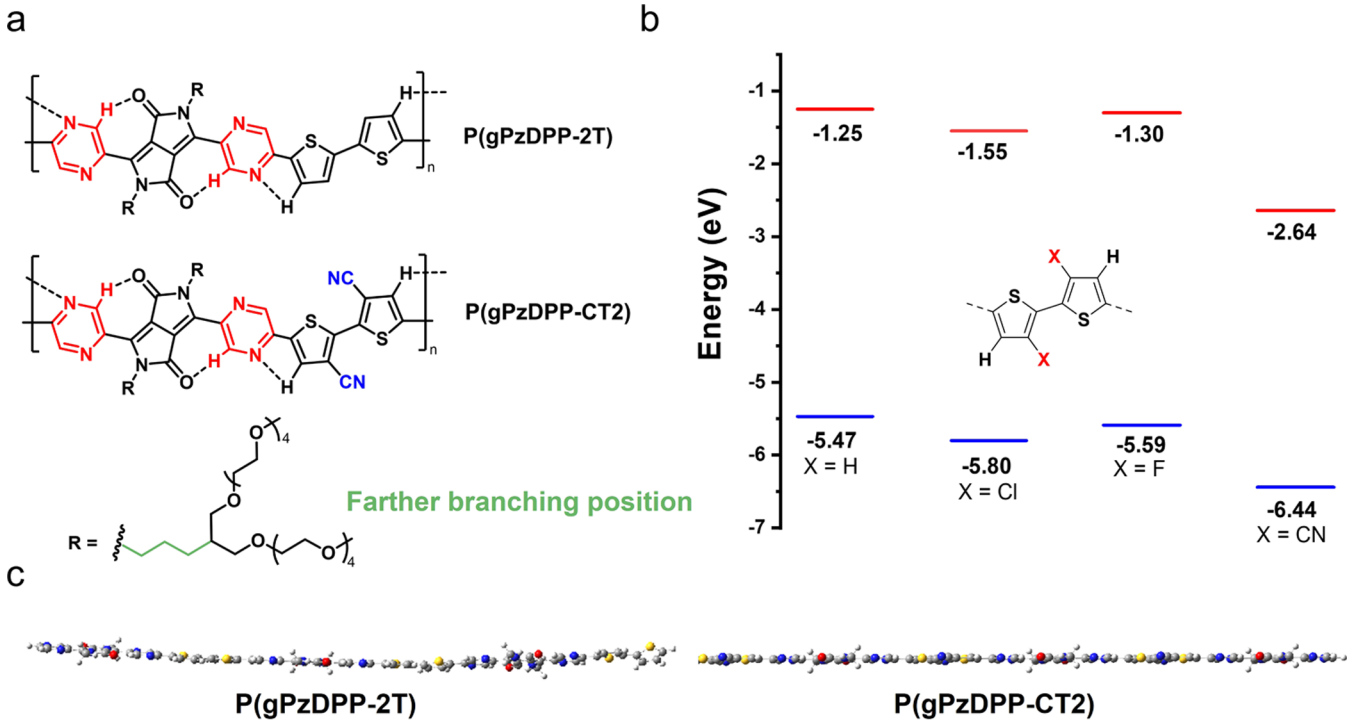

Figure 1. Molecular design strategies for PzDPP polymers. (a) Molecular structures of P(gPzDPP-2T) and P(gPzDPP-CT2). (b) Calculated energy level contrast of four bithiophene grafted with different substituent groups, H, Cl, F, and CN. 3,3′-Dicyano-2,2′-bithiophene has the lowest energy level. (c) Side view of the optimized backbone structures of P(gPzDPP-2T) and P(gPzDPP-CT2).

Scheme 1. Synthetic Routes to the Side Chain and Both Polymers, P(gPzDPP-2T) and P(gPzDPP-CT2)[a]

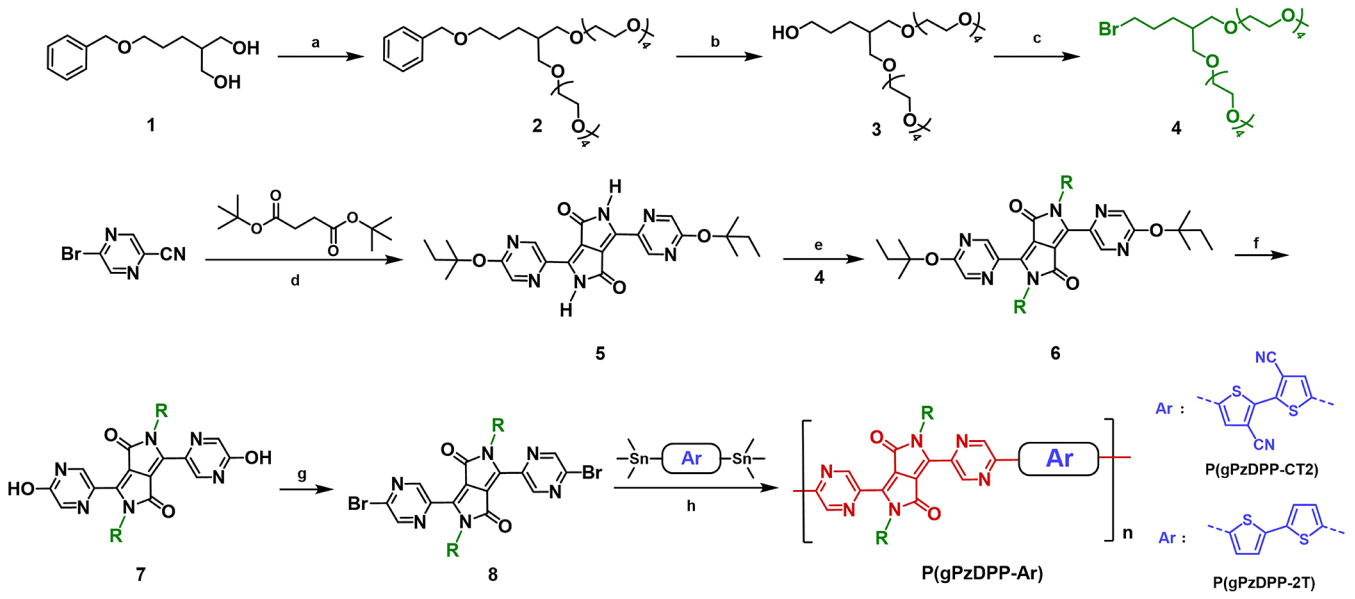

[a]Reagents and Conditions: (a) NaH, THF, 60 °C, 30 min; Add 1 at rt and Then at 65 °C for 12 h. (b) Pd/C, H_2, Ethyl Acetate, rt, 3 Days. (c) PPh_3, DCM, CBr_4, 12 h. (d) Na, $FeCl_3$, *tert*-Amyl Alcohol, 115 °C, 16 h. (e) K_2CO_3, DMF, 12 h. (f) Conc. HCl, 1,4-Dioxane, rt, 4 h. (g) P_2O_5, TBAB, Toluene, 90 °C, 4 h. (h) 5,5-Bis(trimethylstannyl)-3,3′-dicyano-2,2′-bithiophene or 5,5-Bis(trimethylstannyl)-2,2′-bithiophene, $Pd(PPh_3)_4$, CuI, Toluene/NMP, 110 °C, 36 h.

have higher hole mobilities, while the much lower electron mobilities in n-type polymers suggest that the low μ and slow response issue is more serious for n-type OECTs.[21] However, polymers with similar backbone structures for organic field-effect transistors (OFETs) exhibit much higher electron mobility, which is comparable to the p-type ones.[23] McCulloch et al. proved that the polaron delocalization in p-type polymers could impact the charge carrier mobilities.[24] Guo et al. improved the charge carrier mobilities of n-type OECTs ($\sim 10^{-2}$ cm^2 V^{-1} s^{-1}) using fused bithiophene building blocks.[25] To date, only a few works have focused on the strategies to improve the charge carrier mobility of OECTs. Thus, more polymer design approaches are needed to enhance the charge carrier mobility in n-type OECTs.

https://doi.org/10.1021/acs.chemmater.1c04037
Chem. Mater. 2022, 34, 864−872

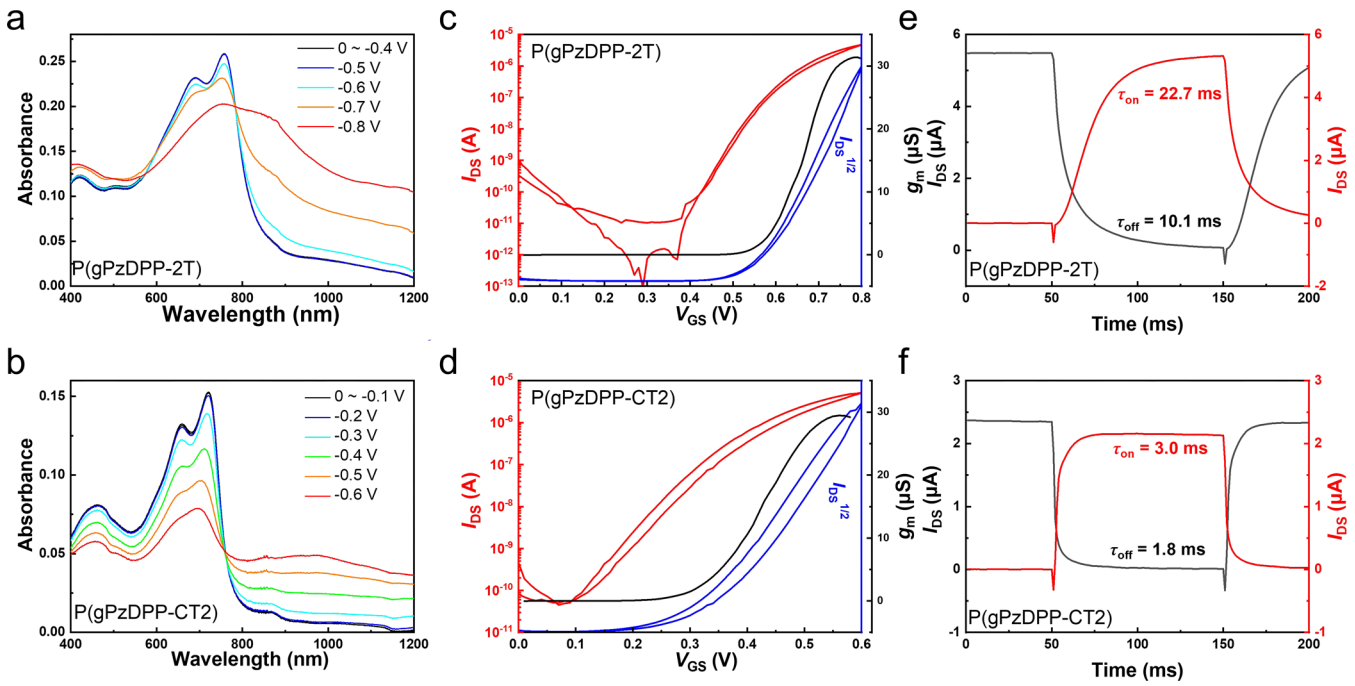

Figure 2. Spectroelectrochemistry and OECT device characterization of P(gPzDPP-2T) and P(gPzDPP-CT2). (a, b) Electrochemical absorption spectra, and (c, d) transfer characteristics of P(gPzDPP-2T) and P(gPzDPP-CT2). W/L = 100/10 μm and V_{DS} = 0.6 V. (e, f) Transient on/off curves with V_{GS} of 0−0.8 and 0−0.6 V for P(gPzDPP-2T) and P(gPzDPP-CT2), respectively. The electrochemical absorption spectra and OECT devices were measured in a 0.1 M NaCl aqueous solution and the gate electrode is a AgCl/Ag pellet.

Here, we demonstrate that introducing electron-withdrawing groups on the donor moiety of D−A polymers could make the negative polaron more distributed on the donor moieties, leading to more delocalized polarons and therefore enhanced electron mobility. With this design, P(gPzDPP-CT2) exhibits a high electron mobility of up to 1.9×10^{-2} cm^2 V^{-1} s^{-1}, 1 order of magnitude higher than the reference polymer. This electron mobility is among the highest in all of the n-type OECT materials. The high electron mobility also leads to a high μC^* of 1.72 F cm^{-1} V^{-1} s^{-1} and short response times of 3.0/1.8 ms, which are the shortest response times in n-type OECT materials.

RESULTS AND DISCUSSION

Diketopyrrolopyrrole (DPP) is one of the most widely used polymer building blocks in high-mobility conjugated polymers.[26] However, all OECT materials based on DPP are p-type, including thiophene-flanked diketopyrrolopyrrole (DPP) and more electron-deficient pyridine-flanked diketopyrrolopyrrole (PyDPP).[24,27,28] Therefore, we chose pyrazine-flanked diketopyrrolopyrrole (PzDPP) as the building block because it has the lowest lowest unoccupied molecular orbital (LUMO) energy level among all reported DPP derivatives.[29] We presumed that after introducing electron-withdrawing groups on the donor moiety, negative polarons would be more distributed on the donor moiety, leading to polaron redistribution. Based on this concept, density functional theory (DFT) calculations were first performed for rational molecular design. We found that the cyano (CN) group has the best effect on reducing the LUMO energy level and also keeping good backbone planarity among four commonly used substituents, H, Cl, F, and CN (Figure 1b).[30] The employment of CN also improved the molecular backbone planarity with a significantly reduced dihedral angle (Figure 1c). We chose the donor units with the highest LUMO energy level (−H) and the lowest LUMO energy level (−CN) to compare the effects of substituents. We designed two PzDPP-based conjugated polymers, namely, P(gPzDPP-2T) and P(gPzDPP-CT2) (Figure 1a). We also designed a new branched ethylene glycol (EG) side chain, which has a branching position far away from the polymer backbone, because we have proved that this kind of farther branched side chain can provide a closer $\pi-\pi$ stacking distance and higher charge carrier mobility.[27]

The synthesis of the new side chain (4) and the two polymers are shown in Scheme 1 (see the Supporting Information for more details). To simplify the synthesis and improve the yield, a new synthetic route was designed for the PzDPP monomer (8). Compared with the previous synthetic procedure, we used di-*tert*-butyl succinate to replace di-isopropyl succinate.[29] This method leads to crude compound 5 that mainly contains *tert*-amyl end groups. To obtain intermediate 7, conc. HCl can be used to remove both alkyl groups without using BBr_3. This step greatly simplifies the synthetic process, and the crude compound can be used for the next step directly. Compound 7 was treated with phosphorus pentoxide and tetrabutylammonium bromide to obtain the bromo-substituted PzDPP (8) for polymerization. Both polymers were obtained via a Pd-catalyzed Stille coupling reaction between 8 and 5,5-bis(trimethylstannyl)-3,3′-dicyano-2,2′-bithiophene or 5,5-bis(trimethylstannyl)-2,2′-bithiophene in the presence of CuI as the cocatalyst. Both polymers were purified by Soxhlet extraction and were finally collected by chloroform. The polymers show high molecular weights over 60 kDa, which were evaluated by gel permeation chromatography (GPC) using hexafluoroisopropanol (HFIP) as the eluent.[27] Both polymers exhibit good thermal stability with high decomposition temperatures (Figure S2).

https://doi.org/10.1021/acs.chemmater.1c04037
Chem. Mater. 2022, 34, 864−872

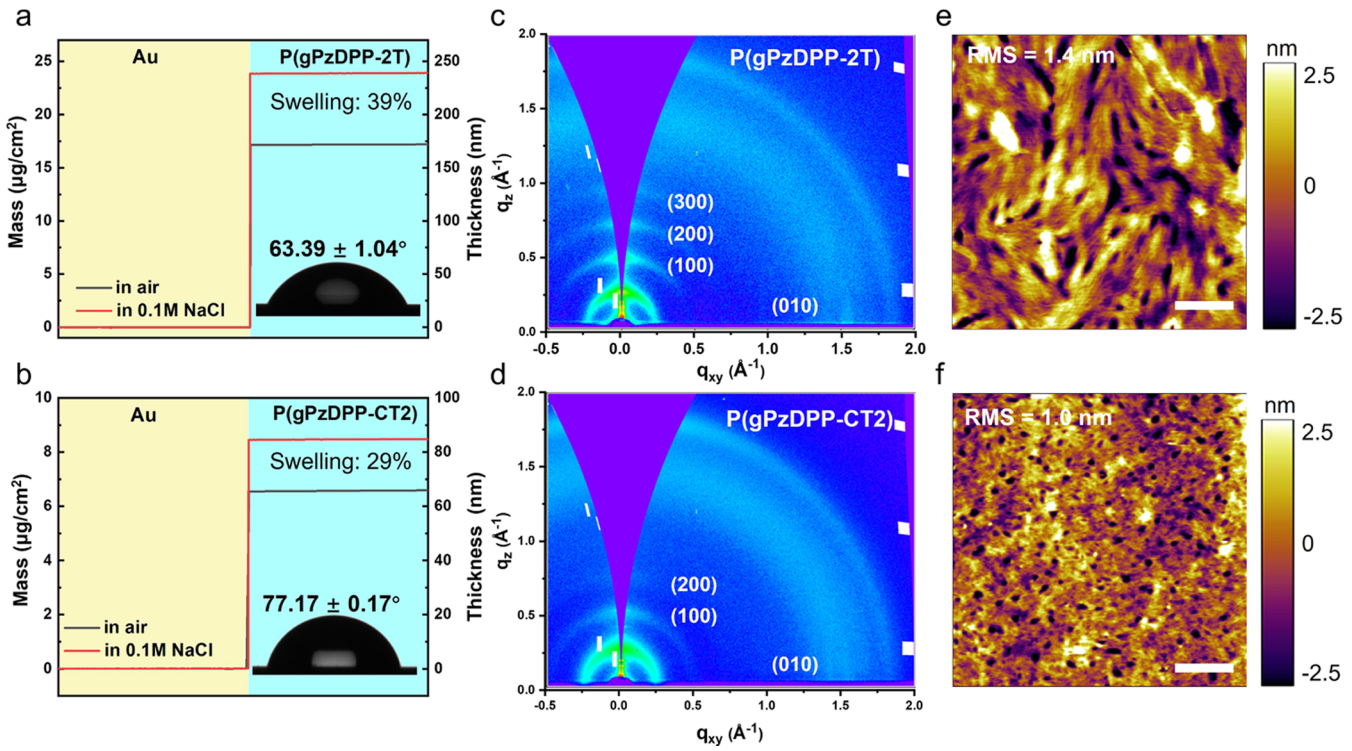

Figure 3. Molecular packing and morphology characteristic of polymers. (a, b) Passive swelling and contact angle with 0.1 M NaCl, for P(gPzDPP-2T) and P(gPzDPP-CT2) films. Swelling degrees are 39% for P(gPzDPP-2T) and 29% for P(gPzDPP-CT2). (c, d) 2D-GIWAXS patterns and (e, f) AFM topography images. The scale bar is 400 nm.

The optoelectronic properties of both polymers were evaluated using ultraviolet−visible−near-infrared (UV−vis−NIR) absorption spectra and cyclic voltammetry (CV). The maximum absorption peak of P(gPzDPP-CT2) in solution shows an obvious blue shift (706 nm) and a larger band gap (1.6 eV) relative to those of P(gPzDPP-T2) (730 nm, 1.65 eV), resulting from less charge transfer from the donor to the acceptor because of the stronger electron-withdrawing property of the CN group (Figure S3). The film spectra show a red shift compared with the solution ones because of polymer aggregation and do not show a significant change after annealing. The measured LUMO energy level of P(gPzDPP-CT2) is −4.19, 0.29 eV lower than that of P(gPzDPP-2T) (Figure S4a, b), which is consistent with the absorption spectroscopy and DFT calculation results (Table S2 and Figure S5).

Continued CV sweep measurements of two polymers were explored in 0.1 M NaCl as the electrolyte (Figure S4c, d). The P(gPzDPP-CT2) film only shows a slight change after the second cycle, while the reduction current decreased continuously for P(gPzDPP-2T), suggesting that P(gPzDPP-CT2) has better electrochemical stability. Spectroelectrochemistry was performed to investigate the electrochemical characteristics of both polymers (Figure 2a,b). A negative voltage was applied to the polymer film on the indium tin oxide (ITO) glass. The applied voltage reduces the polymer and makes the polymer negatively charged. Driven by the negative voltage, sodium ions in the electrolyte penetrate into the polymer film to keep the charge neutrality of the polymer film. The electrochemical doping process generated polarons that show absorption peaks in the long-wavelength region (Figure S6). The absorption spectrum does not change compared to the initial value before the voltage exceeds −0.5 V for P(gPzDPP-2T). For P(gPzDPP-CT2), the spectra begin to change at −0.2 V, which implies its lower operation voltage. With the further increase of bias voltage, the absorption bands (600−800 nm) of the polymers decrease, and the polaron absorption bands (900−1200 nm) increase.

The OECT devices were fabricated using a photolithography and parylene patterning method.[31] The polymers were deposited using their chloroform solution (see the Supporting Information for more details). To evaluate the performance of an OECT material, the following equation based on the Bernards model is often used (eq 1)[32]

$$g_m = (W/L)\cdot d\cdot \mu\cdot C^*\cdot |(V_{th} - V_{GS})| \quad (1)$$

where W, L, and d are the channel width, length, and film thickness, respectively, μ denotes the charge carrier mobility, C^* denotes the capacitance of the channel per unit volume, and V_{th} is the threshold voltage.

Unlike other DPP-based polymers that only exhibited p-type properties, both polymers show typical n-type charge transport behaviors, suggesting that PzDPP is a good building block for n-type OECTs (Figures 2c,d and S7). P(gPzDPP-CT2) shows outstanding OECT performance, with a low V_{th} of 0.32 V and a high μC^* of 1.72 F cm^{-1} V^{-1} s^{-1}. For P(gPzDPP-2T), a 10 times thicker film was prepared for a comparable I_{DS} and g_m due to its much lower μC^* of 0.22 F cm^{-1} V^{-1} s^{-1}. Consistent with the spectroelectrochemistry measurement, the V_{th} of P(gPzDPP-2T) is larger (0.56 V) with a high operation voltage (0.8 V). To further understand the performance differences of the two polymers, the volumetric capacitance (C^*) was measured by the electrochemical impedance spectrum (EIS, Figure S8). Similar to the electrochemical absorption spectra, P(gPzDPP-2T) shows a low volumetric capacitance before a voltage of −0.5 V, while the capacitance of P(gPzDPP-CT2)

https://doi.org/10.1021/acs.chemmater.1c04037
Chem. Mater. 2022, 34, 864−872

Table 1. Summary of the OECT Performance and Molecular Packing Parameters of the Polymers

	g_m[a] (μS)	d (nm)	V_{th}[b] (V)	μC^*_{max}[c] (F/cm V s)	μC^*_{avg}[c] (F/cm V s)	μ[d] (cm^2/V s)	C^* (F cm^{-3})	τ_{on}, τ_{off}[e] (ms)	$d_{lamellar}$ (Å)	$d_{\pi-\pi}$ (Å)	L_c (Å)	g_{lam}	$g_{\pi-\pi}$
P(gPzDPP-2T)	31.4	655	0.56	0.22	0.18	1.6×10^{-3}	134	22.7, 10.1	25.96	3.38	77.67	0.22	0.15
P(gPzDPP-CT2)	29.5	68	0.32	1.72	1.36	1.9×10^{-2}	91	3.0, 1.8	24.83	3.43	49.93	0.27	0.15

[a]The W/L of all devices is 100/10 μm. All of the OECT devices were operated in a 0.1 M NaCl aqueous solution. [b]V_{th} was determined by extrapolating the corresponding $I_{DS}^{1/2}$ versus V_{GS} plots. [c]Six devices were tested and computed for each polymer. μC^* was calculated according to eq 1. [d]μ was calculated from μC^* and the measured volumetric capacitance C^*. [e]The devices for τ_{on} and τ_{off} measurement are independent of the μC^* measurement device.

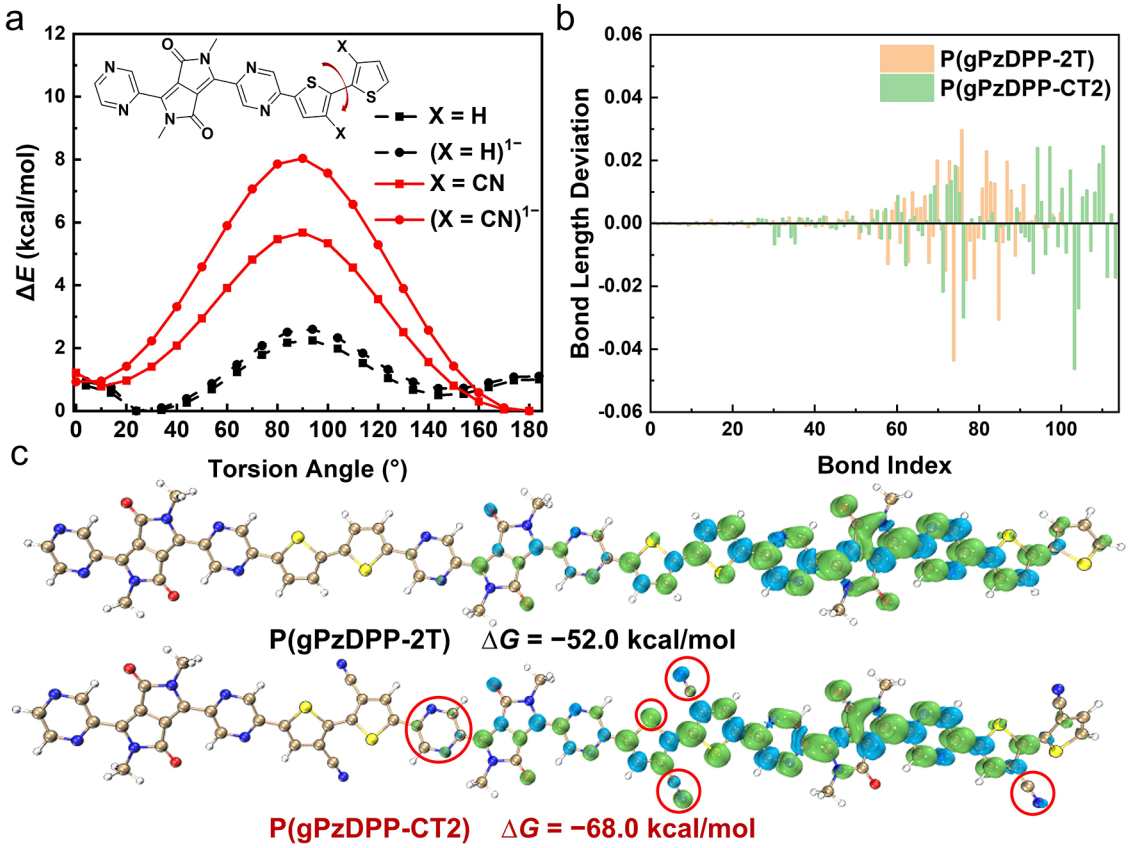

Figure 4. DFT calculations for understanding the charge transport difference in both polymers. (a) Comparison of the relaxed potential energy surface scans of the dihedral angles for the neutral and reduced monomers of P(gPzDPP-2T) and P(gPzDPP-CT2), respectively. (b) Comparison of the bond length deviation of the polaron compared to the neutral state of the polymers. P(gPzDPP-CT2) shows a more delocalized polaron distribution. (c) Spin density distribution of negatively charged P(gPzDPP-2T) and P(gPzDPP-CT2). The red circle markers highlight the major differences in spin density. ΔG stands for the Gibbs free energy change from the neutral to reduced state.

gradually increases with the increase of voltage. The maximal C^* was extracted with average values of 134 F cm^{-3} for P(gPzDPP-2T) and 91 F cm^{-3} for P(gPzDPP-CT2). Based on the μC^* and C^* values, electron mobilities (μ) were calculated to be 1.6×10^{-3} cm^2 V^{-1} s^{-1} for P(gPzDPP-2T) and 1.9×10^{-2} cm^2 V^{-1} s^{-1} for P(gPzDPP-CT2). A 10-fold difference in the electron mobility compensates for the deficiency of capacitance and gains 7.8 times higher μC^*. To evaluate the response speed of both polymers, we tested the transient characteristics of their OECT devices (Figure 2e,f). A 100 ms pulse was applied to the gate electrode, and 0.6 V DC voltage was applied to the drain electrode. The response time was estimated by an exponential fitting of I_{DS}. P(gPzDPP-CT2) exhibits a shorter response time, with a τ_{on} of 3.0 ms and a τ_{off} of 1.8 ms. Besides, the devices of P(gPzDPP-2T) and P(gPzDPP-CT2) show almost the same response time in aqueous solutions with three different electrolytes, NaCl, KCl, and NH_4Cl, which is not proportional to the ion mobility of the cations (Na^+, K^+, and NH_4^+) reported in the literature.[33] Therefore, we believe that ionic mobility has a slight effect on the response speed of the devices in our work (Figures S9 and S10). The high μ and fast response characteristics make P(gPzDPP-CT2) a promising material for real-time high-speed sensing applications. Both polymers show good stability with current retention over ~50% after 100 cycles and 2000 s measurement in air (Figure S11).

Since hydrophilicity is important for ion injection in OECTs,[34] the contact angles of both films were tested. P(gPzDPP-T2) films show an average contact angle of 63.49°, almost 14° smaller than that of P(gPzDPP-CT2). In quartz crystal microbalance with dissipation of energy (QCM-D) measurements, P(gPzDPP-2T) films show 39% swelling during

https://doi.org/10.1021/acs.chemmater.1c04037
Chem. Mater. 2022, 34, 864−872

passive exposure to 0.1 M NaCl, but only 29% for P(gPzDPP-CT2) (Figure 3a,b). This result is consistent with the contact angle measurement, indicating that P(gPzDPP-T2) is more hydrophilic. It is well studied that hydrophilic materials could facilitate ion penetration, which in turn leads to higher volumetric capacitance for OECTs.[17,35] In a recent study, researchers also found that the more hydrophilic n-type OECT polymer with a smaller contact angle exhibited a larger volumetric capacitance, which is consistent with our results.[25] Therefore, the higher volumetric capacitance (C^*) of P(gPzDPP-T2) is largely due to its more hydrophilic film.

Grazing incidence wide-angle X-ray scattering (GIWAXS) was employed to explore the molecular packing (Figures 3c,d and S12). Both polymer films show mixed edge-on and face-on molecular packings. Their lamellar and $\pi-\pi$ stacking distances are listed in Table 1. P(gPzDPP-2T) exhibits three out-of-plane lamellar scattering peaks, (100), (200), and (300), and has a larger coherent length (L_c) and lower paracrystalline disorder (g) in the lamellar direction, suggesting its ordered molecular packing and higher crystallinity. P(gPzDPP-CT2) shows a very similar lamellar distance and slightly larger $\pi-\pi$ stacking distances because both polymers have similar backbones and an identical side chain. Both polymer films are smooth with small root-mean-square (RMS) roughness in atomic force microscopy (AFM) height images (Figure 3e,f). P(gPzDPP-2T) film shows large fibrous zones with higher crystallinity, while P(gPzDPP-CT2) film exhibits a relatively amorphous film, which is consistent with the GIWAXS results. Therefore, the effects of surface roughness, passive swelling, and molecular packing on mobility can be excluded. Thus, the higher charge carrier mobility of P(gPzDPP-CT2) can not be well explained by the film morphology and molecular packing.

To further investigate the reason for the high electron mobility of P(gPzDPP-CT2), DFT calculations were performed. We first performed relaxed potential energy surface (PES) scans at the dihedral angles of the adjacent thiophene units of both polymers (Figure 4a). Compared to the shallow torsional barrier of the thiophene−thiophene (T−T) connection in P(gPzDPP-2T), we found that the cyanothiophene−cyanothiophene (CT−CT) connection in P(gPzDPP-CT2) exhibits a nearly three times higher barrier (Figure 4a). More interestingly, the torsional barrier further increases significantly when P(gPzDPP-CT2) is negatively charged, while it remains low for the negatively charged P(gPzDPP-2T). Therefore, the polymer becomes more planar and rigid after introducing cyano groups, especially under reduced states. We further calculated the Gibbs free energy change and the bond length deviation from the neutral and reduced states for both polymers (three oligomers). P(gPzDPP-CT2) shows a larger Gibbs free energy change (−68.0 kcal/mol), suggesting it is more stable under the reduced state. In addition, P(gPzDPP-CT2) exhibits a longer and more dispersive bond length deviation distribution, implying more delocalized polarons (Figure 4b). This is further supported by the spin density distribution shown in Figure 4c, where the polaron on P(gPzDPP-CT2) is more delocalized. We found that the CN groups make more negative charges distributed on the donor moiety, especially on the S atom of the thiophene and CN groups. The more equalized charge distribution elongates the polaron delocalization length and makes the single bond at the CT−CT connection with more double bond features, which well explains the higher torsional barrier of the reduced state in P(gPzDPP-CT2).

We would like to emphasize that in OECTs, the polymer planarity under the reduced state is more important than that under the neutral state because the polymer is highly charged after electrolyte gating. Previous studies have suggested that polymer packing order is not essential for high-mobility conjugated polymers, especially for D−A polymers.[36] However, the energetic disorder caused by the dihedral angle distribution could have significant influences on charge carrier mobilities.[31] Since lots of counterions and water molecules diffuse into the polymer film after gating, the energetic disorder in OECTs is more severe because ions and water molecules cause more structural and Coulombic disorder.[37] After introducing CN groups, the negative polaron distributes more on the donor moiety, leading to better backbone planarity and rigidity and thereby enhancing the polymer tolerance to the counterion and water-induced disorder. Furthermore, after regulating the negative polaron distribution, the polarons become more delocalized on the polymer backbone, which could also contribute to the higher charge carrier mobility in P(gPzDPP-CT2).

CONCLUSIONS

In summary, we explored the low-performance issue in n-type OECT polymers and found that the low electron mobility is the major issue in limiting their OECT performance and the device response speed. We demonstrate that introducing strong electron-withdrawing groups on the donor moiety can make the polarons more distributed on the donor, leading to more stabilized polarons, enhanced backbone planarity and rigidity, good tolerance to disorder, and finally higher charge carrier mobility. The electron mobility of P(gPzDPP-CT2) in the aqueous environment increased 10 times compared to that of the reference polymer, resulting in a high μC^* of 1.72 F cm^{-1} V^{-1} s^{-1} and short response times of 3.0/1.8 ms. We believe that our polaron regulating strategy could also benefit other n-type OECT polymers, especially for those suffering from the low electron mobility issue.

METHODS

Materials. The synthesis and characterization of the polymers and the various synthetic intermediates are outlined in the Supporting Information.

Spectroelectrochemistry. Spectroelectrochemistry was performed with an ITO-coated glass slide (WE), which was spin-cast with the polymer solution (3×10^{-3} M chloroform solution) at a rotating speed of 500 rpm for 45 s. These polymer-coated ITO slides were employed as the WE and immersed into a cuvette filled with a 0.1 M aqueous NaCl solution, followed by the use of a Pt mesh (CE) and a AgCl/Ag pellet (RE). A PerkinElmer Lambda 750 UV−vis spectrometer was used with the beam path passing through the electrolyte-filled cuvette and polymer-coated ITO samples. A background spectrum with cuvette/electrolyte/ITO was recorded before a potential was applied to the cell. The potential was applied to the WE for 5 s before the spectra were recorded and lasted for a certain period of time until the completion of spectrum scanning.

OECT Fabrication and Characterization. OECT fabrication included the deposition and patterning of metallic electrodes, the parylene layer, and the polymer in the channel. In detail, silica substrates were thoroughly cleaned by ultrasonication in acetone, DI water, and isopropyl alcohol, followed by nitrogen blow drying and brief oxygen plasma cleaning. Metal pads, interconnects, and source/drain contacts were patterned; 5 nm of Cr and 35 nm of Au were subsequently deposited, and then a lift-off process was carried out. Metal interconnects and pads were insulated by depositing 1 μm of parylene-C using a PDS 2010 Labcoater-2, with a 3-(trimethoxysilyl)-

https://doi.org/10.1021/acs.chemmater.1c04037
Chem. Mater. 2022, 34, 864−872

propyl methacrylate (A-174 Silane) adhesion promoter. A 2% aqueous solution of an industrial cleaner (Micro-90) was subsequently spun-coated to act as an antiadhesive for a second sacrificial 1 μm parylene-C film, which was used to simultaneously define the active channel area and to pattern the underlying parylene layer. The samples were subsequently patterned with a 5 μm thick layer of an AZ9260 photoresist and an AZ-400K developer. The patterned areas were opened by reactive ion etching with O_2 plasma using an LCCP-6A reactive ion etcher (Leuven Instruments). The polymer solution was spin-cast on the etched devices with different rotating speeds depending on the desired film thickness. After a peeling-off process of the second sacrificial parylene layer, the OECTs were ready for measurement. The device characterization was performed on a probe station using a Keithley 4200 SCS analyzer. The AgCl/Ag pellet (Warner Instruments) was employed as the gate electrode and immersed into a 0.1 M NaCl solution, which covered the polymer film in the channel. The thickness of the film was determined after a test in a dry state with a DEKTAK profilometer (Bruker).

Electrochemical Impedance Spectra. Electrochemical impedance spectra (EIS) were performed on the polymer-coated electrodes on an electrochemical workstation SP-300 (BioLogic Science Instruments). The polymer film covered on the electrodes was patterned as squares with certain areas by the lithography technique. These polymer-coated electrodes with a glass substrate were employed as the working electrode (WE) and fully covered with a 0.1 M NaCl solution, followed by the employment of the Pt mesh (CE) and the AgCl/Ag pellet (RE) to establish a standard three-electrode system. The capacitances of polymers on electrodes with various sizes were obtained through the potential EIS method, with setting the DC offset voltage as the maximum achievable doping for each polymer. The AC amplitude of voltage in the form of a sine wave on the WE was set as 10 mV (RMS) and the frequency was scanned from 100 kHz to 10 Hz. The as-obtained Bode plots or Nyquist plots were fitted to an equivalent circuit, namely, the Randles circuit Rs (Rp||C), via software EC-Lab view. The thickness of the film was determined after a test in a dry state with a DEKTAK profilometer (Bruker).

Quartz Crystal Microbalance with Dissipation of Energy (QCM-D) Measurements. QCM-D measurements were performed using a Q-sense analyzer (QE401, Biolin Scientific). Passive swelling measurements were performed as follows: First, the QCM-D response of bare Au sensors was recorded in air, followed by injection of a 0.1 M NaCl solution into the chamber. The measurements were then stopped when the f and D were stable, the sensors were removed, and the polymer layers were spin-cast on the same sensors from solutions in chloroform. The absolute f value for each polymer-coated sensor was obtained both in air and in 0.1 M NaCl after the system was in equilibrium. Then, using the function "stitched data" of Q-soft software, the data for multiple overtones between the bare sensor and the polymer-coated sensors were compared both in air and in the electrolyte. Finally, the difference in the f values of the stitched data was directly transformed to the mass absorbed by the polymer (m) in both media, which was calculated by the Sauerbrey equation $\Delta m = -17.7/n \cdot \Delta f_n$, where n is the overtone number. The fifth overtone was used in this research. The thickness of the polymer was estimated with a density of 1 g/cm^3.

Contact Angle Measurements. Contact angle measurements were performed using an optical contact angle measuring device based on the pendant drop method (KRÜSS drop shape analyzer DSA30, Germany). The polymers were spin-coated on SiO_2 substrates, and the electrolyte was 0.1 M NaCl.

DFT Calculations. Geometry optimization, molecular energy level calculation, and relaxed potential energy surface scan were performed at the B3LYP/6-311g(d,p) or wB97XD/6-311g(d,p) level using Gaussian 16 and Gaussian View 6.[31,38] The computation results were visualized by Multiwfn[39] and VMD.[40] Using C* from EIS and lattice parameters from GIWAXS, we can estimate that 3−4 segments share one electron for P(gPzDPP-2T) and P(gPzDPP-CT2). Therefore, the bond length deviation of the neutral and reduced states was calculated for three segments. For absorption spectra calculation, td(nstates = 50) were used for the oligomers (n = 2).

AFM and GIWAXS Characterization. Atomic force microscopy (AFM) measurements were performed with a Cypher atomic force microscope (Asylum Research, Oxford Instruments). The surface morphology was recorded with a scan rate of 1−2 Hz at the AC mode. The GIWAXS experiment was performed on the Xenocs Xuess 2.0 beamline, with an incident X-ray angle of 0.2° and a wavelength of 1.54 Å. The scattered signal was collected using a PILATUS 1M detector at a sample-to-detector distance of 150 mm. Data processing was performed by Igor Pro software with Nika and WAXTools packages. Coherence length (L_c) was calculated from the breadth (Δq) of a diffraction peak: $L_c = 0.89 \times 2\pi/\Delta q$.[36,41] Paracrystalline disorder was calculated from the center position (q_0) and the breadth (Δq) of a diffraction peak: $g = (\Delta q/(2\pi q_0))^{1/2}$.[36,41]

■ ASSOCIATED CONTENT

Supporting Information

The Supporting Information is available free of charge at https://pubs.acs.org/doi/10.1021/acs.chemmater.1c04037.

Synthesis and characterization of the polymers; ^{1}H and ^{13}C{^{1}H} NMR spectra; TGA traces; UV−vis−NIR absorption spectra; cyclic voltammograms; DFT simulations; OECT characterization plots; and GIWAXS line cuts (PDF)

■ AUTHOR INFORMATION

Corresponding Author

Ting Lei − *Key Laboratory of Polymer Chemistry and Physics of Ministry of Education, School of Materials Science and Engineering, Peking University, Beijing 100871, China;* orcid.org/0000-0001-8190-9483; Email: tinglei@pku.edu.cn

Authors

Junwei Shi − *Key Laboratory of Polymer Chemistry and Physics of Ministry of Education, School of Materials Science and Engineering, Peking University, Beijing 100871, China; Beijing National Laboratory for Molecular Science, College of Chemistry and Molecular Engineering, Peking University, Beijing 100871, China*

Peiyun Li − *Key Laboratory of Polymer Chemistry and Physics of Ministry of Education, School of Materials Science and Engineering, Peking University, Beijing 100871, China;* orcid.org/0000-0001-7805-527X

Xin-Yu Deng − *Key Laboratory of Polymer Chemistry and Physics of Ministry of Education, School of Materials Science and Engineering, Peking University, Beijing 100871, China*

Jingcao Xu − *Key Laboratory of Polymer Chemistry and Physics of Ministry of Education, School of Materials Science and Engineering, Peking University, Beijing 100871, China*

Zhen Huang − *Beijing National Laboratory for Molecular Science, College of Chemistry and Molecular Engineering, Peking University, Beijing 100871, China*

Yuqiu Lei − *College of Engineering, Peking University, Beijing 100871, China*

Yunfei Wang − *School of Polymer Science and Engineering, The University of Southern Mississippi, Hattiesburg, Mississippi 39406, USA;* orcid.org/0000-0001-7555-5308

Jie-Yu Wang − *Beijing National Laboratory for Molecular Science, College of Chemistry and Molecular Engineering, Peking University, Beijing 100871, China;* orcid.org/0000-0002-1903-8928

https://doi.org/10.1021/acs.chemmater.1c04037
Chem. Mater. 2022, 34, 864−872

Xiaodan Gu − *School of Polymer Science and Engineering, The University of Southern Mississippi, Hattiesburg, Mississippi 39406, USA;* orcid.org/0000-0002-1123-3673

Complete contact information is available at: https://pubs.acs.org/10.1021/acs.chemmater.1c04037

Author Contributions

†J.S. and P.L. contributed equally to this work.

Notes

The authors declare no competing financial interest.

■ ACKNOWLEDGMENTS

This work was supported by the National Natural Science Foundation of China (92156019 and 22075001) and the Open Fund of the State Key Laboratory of Luminescent Materials and Devices, South China University of Technology (2021-skllmd-02). T.L. thanks the Clinical Medicine Plus X-Young Scholars Project, Peking University, the Fundamental Research Funds for the Central Universities. J.S. thanks the China Postdoctoral Science Foundation (2020M680190) and the Boya Postdoctoral Fellowship of Peking University. Y.W. and X.G. thanks the Department of Energy for providing supports to enable the scattering experiments in this work. The computational part is supported by High-Performance Computing Platform of Peking University. The authors thank Xiaodong Lian and Yapei Wang from Renmin University of China for their help in contact angle measurement.

■ REFERENCES

(1) Pappa, A. M.; Curto, V. F.; Braendlein, M.; Strakosas, X.; Donahue, M. J.; Fiocchi, M.; Malliaras, G. G.; Owens, R. M. Organic Transistor Arrays Integrated with Finger-Powered Microfluidics for Multianalyte Saliva Testing. *Adv. Healthcare Mater.* **2016**, *5*, 2295−2302.

(2) Williamson, A.; Ferro, M.; Leleux, P.; Ismailova, E.; Kaszas, A.; Doublet, T.; Quilichini, P.; Rivnay, J.; Rozsa, B.; Katona, G.; Bernard, C.; Malliaras, G. G. Localized Neuron Stimulation with Organic Electrochemical Transistors on Delaminating Depth Probes. *Adv. Mater.* **2015**, *27*, 4405−4410.

(3) van de Burgt, Y.; Lubberman, E.; Fuller, E. J.; Keene, S. T.; Faria, G. C.; Agarwal, S.; Marinella, M. J.; Alec Talin, A.; Salleo, A. A Non-Volatile Organic Electrochemical Device as a Low-Voltage Artificial Synapse for Neuromorphic Computing. *Nat. Mater.* **2017**, *16*, 414−418.

(4) Rivnay, J.; Inal, S.; Salleo, A.; Owens, R. M.; Berggren, M.; Malliaras, G. G. Organic Electrochemical Transistors. *Nat. Rev. Mater.* **2018**, *3*, No. 17086.

(5) Zeglio, E.; Inganas, O. Active Materials for Organic Electrochemical Transistors. *Adv. Mater.* **2018**, *30*, No. e1800941.

(6) Chen, S.; Surendran, A.; Wu, X.; Lee, S. Y.; Stephen, M.; Leong, W. L. Recent Technological Advances in Fabrication and Application of Organic Electrochemical Transistors. *Adv. Mater. Technol.* **2020**, *5*, No. 2000523.

(7) Nielsen, C. B.; Giovannitti, A.; Sbircea, D. T.; Bandiello, E.; Niazi, M. R.; Hanifi, D. A.; Sessolo, M.; Amassian, A.; Malliaras, G. G.; Rivnay, J.; McCulloch, I. Molecular Design of Semiconducting Polymers for High-Performance Organic Electrochemical Transistors. *J. Am. Chem. Soc.* **2016**, *138*, 10252−10259.

(8) Moser, M.; Hidalgo, T. C.; Surgailis, J.; Gladisch, J.; Ghosh, S.; Sheelamanthula, R.; Thiburce, Q.; Giovannitti, A.; Salleo, A.; Gasparini, N.; Wadsworth, A.; Zozoulenko, I.; Berggren, M.; Stavrinidou, E.; Inal, S.; McCulloch, I. Side Chain Redistribution as a Strategy to Boost Organic Electrochemical Transistor Performance and Stability. *Adv. Mater.* **2020**, *32*, No. e2002748.

(9) Wang, Y.; Zeglio, E.; Liao, H.; Xu, J.; Liu, F.; Li, Z.; Maria, I. P.; Mawad, D.; Herland, A.; McCulloch, I.; Yue, W. Hybrid Alkyl−Ethylene Glycol Side Chains Enhance Substrate Adhesion and Operational Stability in Accumulation Mode Organic Electrochemical Transistors. *Chem. Mater.* **2019**, *31*, 9797−9806.

(10) Wu, X.; Liu, Q.; Surendran, A.; Bottle, S. E.; Sonar, P.; Leong, W. L. Enhancing the Electrochemical Doping Efficiency in Diketopyrrolopyrrole-Based Polymer for Organic Electrochemical Transistors. *Adv. Electron. Mater.* **2021**, *7*, No. 2000701.

(11) Hallani, R. K.; Paulsen, B. D.; Petty, A. J., 2nd; Sheelamanthula, R.; Moser, M.; Thorley, K. J.; Sohn, W.; Rashid, R. B.; Savva, A.; Moro, S.; Parker, J. P.; Drury, O.; Alsufyani, M.; Neophytou, M.; Kosco, J.; Inal, S.; Costantini, G.; Rivnay, J.; McCulloch, I. Regiochemistry-Driven Organic Electrochemical Transistor Performance Enhancement in Ethylene Glycol-Functionalized Polythiophenes. *J. Am. Chem. Soc.* **2021**, *143*, 11007−11018.

(12) Luo, X.; Shen, H.; Perera, K.; Tran, D. T.; Boudouris, B. W.; Mei, J. Designing Donor−Acceptor Copolymers for Stable and High-Performance Organic Electrochemical Transistors. *ACS Macro Lett.* **2021**, *10*, 1061−1067.

(13) Sun, H.; Gerasimov, J.; Berggren, M.; Fabiano, S. N-Type Organic Electrochemical Transistors: Materials and Challenges. *J. Mater. Chem. C* **2018**, *6*, 11778−11784.

(14) Griggs, S.; Marks, A.; Bristow, H.; McCulloch, I. N-Type Organic Semiconducting Polymers: Stability Limitations, Design Considerations and Applications. *J. Mater. Chem. C* **2021**, *9*, 8099−8128.

(15) Giovannitti, A.; Nielsen, C. B.; Sbircea, D. T.; Inal, S.; Donahue, M.; Niazi, M. R.; Hanifi, D. A.; Amassian, A.; Malliaras, G. G.; Rivnay, J.; McCulloch, I. N-Type Organic Electrochemical Transistors with Stability in Water. *Nat. Commun.* **2016**, *7*, No. 13066.

(16) Sun, H.; Vagin, M.; Wang, S.; Crispin, X.; Forchheimer, R.; Berggren, M.; Fabiano, S. Complementary Logic Circuits Based on High-Performance N-Type Organic Electrochemical Transistors. *Adv. Mater.* **2018**, *30*, No. 1704916.

(17) Chen, X.; Marks, A.; Paulsen, B. D.; Wu, R.; Rashid, R. B.; Chen, H.; Alsufyani, M.; Rivnay, J.; McCulloch, I. N-Type Rigid Semiconducting Polymers Bearing Oligo(Ethylene Glycol) Side Chains for High-Performance Organic Electrochemical Transistors. *Angew. Chem., Int. Ed.* **2021**, *60*, 9368−9373.

(18) Giovannitti, A.; Maria, I. P.; Hanifi, D.; Donahue, M. J.; Bryant, D.; Barth, K. J.; Makdah, B. E.; Savva, A.; Moia, D.; Zetek, M.; Barnes, P. R. F.; Reid, O. G.; Inal, S.; Rumbles, G.; Malliaras, G. G.; Nelson, J.; Rivnay, J.; McCulloch, I. The Role of the Side Chain on the Performance of N-Type Conjugated Polymers in Aqueous Electrolytes. *Chem. Mater.* **2018**, *30*, 2945−2953.

(19) Romele, P.; Gkoupidenis, P.; Koutsouras, D. A.; Lieberth, K.; Kovacs-Vajna, Z. M.; Blom, P. W. M.; Torricelli, F. Multiscale Real Time and High Sensitivity Ion Detection with Complementary Organic Electrochemical Transistors Amplifier. *Nat. Commun.* **2020**, *11*, No. 3743.

(20) Li, P. Y.; Lei, T. Molecular Design Strategies for High-Performance Organic Electrochemical Transistors. *J. Polym. Sci.* **2021**, DOI: 10.1002/pol.20210503.

(21) Cea, C.; Spyropoulos, G. D.; Jastrzebska-Perfect, P.; Ferrero, J. J.; Gelinas, J. N.; Khodagholy, D. Enhancement-Mode Ion-Based Transistor as a Comprehensive Interface and Real-Time Processing Unit for in Vivo Electrophysiology. *Nat. Mater.* **2020**, *19*, 679−686.

(22) Spyropoulos, G. D.; Gelinas, J. N.; Khodagholy, D. Internal Ion-Gated Organic Electrochemical Transistor: A Building Block for Integrated Bioelectronics. *Sci. Adv.* **2019**, *5*, No. eaau7378.

(23) Chen, Z.; Zheng, Y.; Yan, H.; Facchetti, A. Naphthalenedicarboximide- Vs Perylenedicarboximide-Based Copolymers. Synthesis and Semiconducting Properties in Bottom-Gate N-Channel Organic Transistors. *J. Am. Chem. Soc.* **2009**, *131*, 8−9.

(24) Moser, M.; Savva, A.; Thorley, K.; Paulsen, B. D.; Hidalgo, T. C.; Ohayon, D.; Chen, H.; Giovannitti, A.; Marks, A.; Gasparini, N.; Wadsworth, A.; Rivnay, J.; Inal, S.; McCulloch, I. Polaron

Delocalization in Donor-Acceptor Polymers and Its Impact on Organic Electrochemical Transistor Performance. *Angew. Chem., Int. Ed.* **2021**, *60*, 7777−7785.
(25) Feng, K.; Shan, W.; Ma, S.; Wu, Z.; Chen, J.; Guo, H.; Liu, B.; Wang, J.; Li, B.; Woo, H. Y.; Fabiano, S.; Huang, W.; Guo, X. Fused Bithiophene Imide Dimer-Based N-Type Polymers for High-Performance Organic Electrochemical Transistors. *Angew. Chem., Int. Ed.* **2021**, *60*, 24198−24205.
(26) Yang, J.; Zhao, Z.; Wang, S.; Guo, Y.; Liu, Y. Insight into High-Performance Conjugated Polymers for Organic Field-Effect Transistors. *Chem* **2018**, *4*, 2748−2785.
(27) Jia, H.; Huang, Z.; Li, P.; Zhang, S.; Wang, Y.; Wang, J.-Y.; Gu, X.; Lei, T. Engineering Donor−Acceptor Conjugated Polymers for High-Performance and Fast-Response Organic Electrochemical Transistors. *J. Mater. Chem. C* **2021**, *9*, 4927−4934.
(28) Giovannitti, A.; Rashid, R. B.; Thiburce, Q.; Paulsen, B. D.; Cendra, C.; Thorley, K.; Moia, D.; Mefford, J. T.; Hanifi, D.; Weiyuan, D.; Moser, M.; Salleo, A.; Nelson, J.; McCulloch, I.; Rivnay, J. Energetic Control of Redox-Active Polymers toward Safe Organic Bioelectronic Materials. *Adv. Mater.* **2020**, *32*, No. e1908047.
(29) Yan, X.; Xiong, M.; Li, J. T.; Zhang, S.; Ahmad, Z.; Lu, Y.; Wang, Z. Y.; Yao, Z. F.; Wang, J. Y.; Gu, X.; Lei, T. Pyrazine-Flanked Diketopyrrolopyrrole (Dpp): A New Polymer Building Block for High-Performance N-Type Organic Thermoelectrics. *J. Am. Chem. Soc.* **2019**, *141*, 20215−20221.
(30) Ding, B.; Kim, G.; Kim, Y.; Eisner, F. D.; Gutierrez-Fernandez, E.; Martin, J.; Yoon, M. H.; Heeney, M. Influence of Backbone Curvature on the Organic Electrochemical Transistor Performance of Glycolated Donor-Acceptor Conjugated Polymers. *Angew. Chem., Int. Ed.* **2021**, *60*, 19679−19684.
(31) Dennington, Roy.; Keith, Todd A.; Millam, John M. GaussView V. Semichem Inc.: Shawnee Mission, KS, 2016.
(32) Bernards, D. A.; Malliaras, G. G. Steady-State and Transient Behavior of Organic Electrochemical Transistors. *Adv. Funct. Mater.* **2007**, *17*, 3538−3544.
(33) Pethig, R. Dielectric-Properties of Biological-Materials - Biophysical and Medical Applications. *IEEE Trans. Electr. Insul.* **1984**, *EI-19*, 453−474.
(34) Savva, A.; Cendra, C.; Giugni, A.; Torre, B.; Surgailis, J.; Ohayon, D.; Giovannitti, A.; McCulloch, I.; Di Fabrizio, E.; Salleo, A.; Rivnay, J.; Inal, S. Influence of Water on the Performance of Organic Electrochemical Transistors. *Chem. Mater.* **2019**, *31*, 927−937.
(35) Giovannitti, A.; Sbircea, D. T.; Inal, S.; Nielsen, C. B.; Bandiello, E.; Hanifi, D. A.; Sessolo, M.; Malliaras, G. G.; McCulloch, I.; Rivnay, J. Controlling the Mode of Operation of Organic Transistors through Side-Chain Engineering. *Proc. Natl. Acad. Sci. U.S.A.* **2016**, *113*, 12017−12022.
(36) Noriega, R.; Rivnay, J.; Vandewal, K.; Koch, F. P.; Stingelin, N.; Smith, P.; Toney, M. F.; Salleo, A. A General Relationship between Disorder, Aggregation and Charge Transport in Conjugated Polymers. *Nat. Mater.* **2013**, *12*, 1038−1044.
(37) Friedlein, J. T.; Rivnay, J.; Dunlap, D. H.; McCulloch, I.; Shaheen, S. E.; McLeod, R. R.; Malliaras, G. G. Influence of Disorder on Transfer Characteristics of Organic Electrochemical Transistors. *Appl. Phys. Lett.* **2017**, *111*, No. 023301.
(38) Frisch, M. J.; Trucks, G. W.; Schlegel, H. B.; Scuseria, G. E.; Robb, M. A.; Cheeseman, J. R.; Scalmani, G.; Barone, V.; Petersson, G. A.; Nakatsuji, H.; Li, X.; Caricato, M.; Marenich, A. V.; Bloino, J.; Janesko, B. G.; Gomperts, R.; Mennucci, B.; Hratchian, H. P.; Ortiz, J. V.; Izmaylov, A. F.; Sonnenberg, J. L.; Williams; Ding, F.; Lipparini, F.; Egidi, F.; Goings, J.; Peng, B.; Petrone, A.; Henderson, T.; Ranasinghe, D.; Zakrzewski, V. G.; Gao, J.; Rega, N.; Zheng, G.; Liang, W.; Hada, M.; Ehara, M.; Toyota, K.; Fukuda, R.; Hasegawa, J.; Ishida, M.; Nakajima, T.; Honda, Y.; Kitao, O.; Nakai, H.; Vreven, T.; Throssell, K.; Montgomery, J. A., Jr; Peralta, J. E.; Ogliaro, F.; Bearpark, M. J.; Heyd, J. J.; Brothers, E. N.; Kudin, K. N.; Staroverov, V. N.; Keith, T. A.; Kobayashi, R.; Normand, J.; Raghavachari, K.; Rendell, A. P.; Burant, J. C.; Iyengar, S. S.; Tomasi, J.; Cossi, M.; Millam, J. M.; Klene, M.; Adamo, C.; Cammi, R.; Ochterski, J. W.; Martin, R. L.; Morokuma, K.; Farkas, O.; Foresman, J. B.; Fox, D. J.. *Gaussian 16*, Rev. C.01, Gaussian 16: Wallingford CT %!, 2016.
(39) Lu, T.; Chen, F. Multiwfn: A Multifunctional Wavefunction Analyzer. *J. Comput. Chem.* **2012**, *33*, 580−592.
(40) Humphrey, W.; Dalke, A.; Schulten, K. Vmd: Visual Molecular Dynamics. *J. Mol. Graphics* **1996**, *14*, 33−38.
(41) Rivnay, J.; Noriega, R.; Kline, R. J.; Salleo, A.; Toney, M. F. Quantitative Analysis of Lattice Disorder and Crystallite Size in Organic Semiconductor Thin Films. *Phys. Rev. B* **2011**, *84*, No. 045203.

https://doi.org/10.1021/acs.chemmater.1c04037
Chem. Mater. 2022, 34, 864−872